Available online at www.sciencedirect.com
ScienceDirect
Journal of Catalysis 251 (2007) 321–331
JOURNAL OF CATALYSIS
www.elsevier.com/locate/jcat

Electronic and structural promotion of barium hexaaluminate as a ruthenium catalyst support for ammonia synthesis

Zhixiong You, Koji Inazu, Ken-ichi Aika, Toshihide Baba *

Department of Environmental Chemistry and Engineering, Interdisciplinary Graduate School of Science and Technology, Tokyo Institute of Technology, G1-14 4259 Nagatsuta, Midori-ku, Yokohama 226-8502, Japan

Received 4 June 2007; revised 4 August 2007; accepted 7 August 2007

Available online 21 September 2007

Abstract

Barium hexaaluminate (BHA) with large surface area (49 $m^2\ g^{-1}$) is synthesized by microemulsion-mediated synthesis technique and examined as a support promoting ammonia synthesis by particulate Ru. The Ru/BHA catalyst exhibits higher activity and stability than Ba-promoted Ru/MgO, the previously most active oxide-supported catalyst system for ammonia synthesis. The rate of ammonia synthesis over Ru/BHA is 5426 μmol $g_{cat}^{-1}\ h^{-1}$ (653 K, 1.1 MPa), more than twice of that of Ba–Ru/MgO, and no decrease in the rate is observed over reaction for 80 h at 653 K and 0.1 MPa. Characterization of this catalyst system by various techniques reveals that the electronic and structural interactions between BHA and Ru particles are key factors responsible for the elevated activity and stability of this catalyst.

Keywords: Ammonia synthesis; Ruthenium catalyst; Barium hexaaluminate; Electronic promotion; Structural promotion

1. Introduction

Ruthenium catalysts have been investigated extensively as the second-generation catalysts for ammonia synthesis, providing higher activity at lower temperatures and pressures compared with conventional iron catalysts [1–11]. The activity of Ru catalysts strongly depends on the properties of the supports as well as on the nature of the catalysis promoters [6,10,12]. Among the wide range of supports investigated for Ru catalysts, including carbon [1,2,4,13–15], MgO [7–9,16], Al_2O_3 [4,5,12, 17–20], zeolite X [21–23], CeO_2 [24], $MgAl_2O_4$ [25], and BN [11,26], the Ru/C system exhibits the highest activity for ammonia synthesis. Ruthenium/carbon catalysts have already been applied industrially in the Kellog Brown & Root advanced ammonia process (KBRAAP) [27,28]; however, carbon supports react readily with H_2 (one reactant of ammonia synthesis) to form methane in the presence of Ru under the conditions of ammonia synthesis. Methanation in this manner causes gradual degradation of the carbon support, limiting the lifetime of the Ru/C catalyst [29–31]. The combustible nature of carbon also constrains its use in practical processes as a safe catalytic support.

It is thus desirable to develop a new oxide support for Ru catalysts that overcomes these issues. Magnesium oxide is currently the most suitable oxide support for Ru catalysts due to its low acidity [32], but its high reactivity to H_2O and low textural stability [28,33] inhibit its widespread use in industry. As acid sites consume available Ru electrons, the high acidity of Al_2O_3 and zeolite has a detrimental effect on the activity of Ru catalysts [20]. Therefore, the development of a suitable oxide support for Ru catalysts remains a significant challenge.

In ammonia synthesis reactions over Ru catalysts, the rate-determining step is the dissociation of N_2 molecules on the surface of Ru particles [34], which is known to be structure-sensitive [35]. Dahl et al. have proven that the active site for N_2 dissociation is the B_5 site, which consists of five Ru atoms: two at step edges and three on the lower terrace [35–38]. The abundance of B_5 sites depends on the size and shape of the Ru particles, which are influenced by the structure and morphology of the support, as well as by the kind of Ru precursor and Ru loading. Ruthenium is present as round particles on most

* Corresponding author. Fax: +81 45 924 5480.
E-mail address: tbaba@chemenv.titech.ac.jp (T. Baba).

0021-9517/$ – see front matter
doi:10.1016/j.jcat.2007.08.006

supports, including carbon (both partially graphitized and non-graphitized), BN, MgO, $MgAl_2O_4$, Al_2O_3, and zeolite X [35, 39–42]. With such a round shape, the activity of Ru catalysts for ammonia synthesis has been found to increase with the size of Ru particles up to a saturated maximum for particles 5 nm in diameter [41]. In addition to size tuning, changing the shape of Ru particles also can increase the abundance of B_5 sites. Song et al. [15] have reported that flat Ru particles are more active for the dissociative adsorption of N_2 molecules than round particles, due to the higher density of B_5 sites on the flat particle surfaces. They thus concluded that the high activity of the Ru/C system is attributable to the flat Ru particles grown epitaxially on the layered structure of graphitized carbon support.

The electronic properties of Ru particles also can be modified by the support. Ruthenium catalysts supported on basic oxides, such as MgO, are reported to be more active for ammonia synthesis than those supported on acidic oxides, such as γ-Al_2O_3 [15,19]. Moreover, the addition of a basic promoter (e.g., alkali or alkaline earth compounds) to the Ru catalysts has been found experimentally to result in dramatically enhanced activity for ammonia synthesis [4,19], likely due to an electronic promotion effect of the support or promoter. To explain this electronic promotion effect, Aika et al. [5] proposed a detailed mechanism in which electrons are transferred from the support or promoter to Ru metal, resulting in a decreased ionization potential of Ru, thereby allowing electron transfer from the metal to the antibonding orbits of the N atom and reducing the activation energy for the dissociative adsorption of N_2 molecules. Dahl et al. [32] further suggested that the donated negative charge might destabilize the adsorption of NH* (the intermediate form of NH_3) on Ru and relax its competing adsorption with N_2. Based on density functional theory (DFT) calculations, Logadóttir and Nørskov also suggested that the promotional effect of alkali metals results from a combination of stabilization of the transition state of N_2 dissociation and destabilization of NH* on Ru [43]. DFT calculations have shown that the effect of the promoter is based on the electrostatic interaction between the adsorption-induced dipole moment and the electrostatic field induced by the promoter.

Previous studies have clearly shown that the support influences the activity of Ru particles both structurally and electronically. Therefore, an ideal support for Ru catalysts should promote the catalytic performance of Ru particles both electronically and structurally. Our group recently synthesized Ba- or Cs-modified alumina using a reverse-microemulsion-mediated synthesis technique; the resulting supports exhibited both improved thermal stability (due to the presence of large Ba^{2+} or Cs^+ cations [44–46]) and modified acid properties [47]. These results indicate that Ba- or Cs-modified alumina may be a promising support for Ru catalysts. In the present report, Ru on a Ba-modified alumina composite, barium hexaaluminate (BHA), is demonstrated to exhibit superior activity and stability for ammonia synthesis, and the factors responsible for this enhanced catalytic performance are examined at length.

2. Experimental

2.1. Preparation of BHA support

BHA was prepared by a reverse microemulsion-mediated synthesis technique reported previously [44,46], to obtain a product with high surface area. This technique involved preparing a stable and transparent microemulsion system by mixing 70 mL of distilled water, 30 mL of polyethylene glycol 200 (PEG 200, Wako), ca. 360 mL of *n*-propanol (Wako), and 190 mL of isooctane (2,2,4-trimethylpentane, Aldrich). To this emulsion was added a precursor solution prepared by dissolving 2.571 g of aluminum isopropoxide (Aldrich) and 0.268 g of barium isopropoxide (Aldrich) (Ba/Al = 1/12 by mol) in 20 mL of ethyl acetoacetate at 353 K, followed by the addition of 20 mL of isooctane. After hydrolization of the alkoxides by stirring under ambient conditions for 20 h, the hydrolyzed mixture was transferred into an autoclave and treated hydrothermally at 423 K for 20 h. The nanocomposite thus produced was recovered by evaporating the solvents and then decomposing the surfactant at 773 K for 2 h. The sample was finally calcined at 1373 K for 24 h to obtain the BHA support with a typical surface area of 49 $m^2\,g^{-1}$.

2.2. Preparation of supported Ru catalysts

Ruthenium catalysts were prepared by impregnating the calcined BHA support using a tetrahydrofuran (THF) solution containing $Ru_3(CO)_{12}$. The solution was stirred under ambient conditions for 6 h, after which the THF solvent was removed by treatment in a rotary evaporator under reduced pressure at room temperature. After drying in air at 383 K for 12 h, the sample was treated in a vacuum (ca. 10^{-4} Pa) at 673 K for 3 h to decompose the $Ru_3(CO)_{12}$. The catalyst thus obtained ("as-prepared") had a nominal Ru content of 8 wt% and a calculated Ba-to-Ru molar ratio of 1.6.

For comparison with other oxide supports, Ru/γ-Al_2O_3 (Aerosil, Japan) and Ru/MgO (Soekawa Chemicals, Japan) were also prepared at a Ru content of 8 wt% using the same impregnation and calcination procedures. Parts of the Ru/γ-Al_2O_3 and Ru/MgO catalysts were also impregnated with Ba promoter by immersion in an aqueous solution of $Ba(NO_3)_2$ and then dried at 383 K to give catalysts with a Ba-to-Ru molar ratio of 1.6 (as for Ru/BHA).

2.3. Ammonia synthesis

Ammonia synthesis reactions were carried out in a fixed-bed flow system under computer control. Before reactions, all samples were pelletized, crushed, and sieved. The 300–600 μm fractions were collected and loaded into a stainless steel tubular reactor. Before activity tests, the samples were treated under H_2 flow at 473 K for 1 h to reduce Ru to the metallic state, and then for a further 3 h at 773 K to decompose $Ba(NO_3)_2$.

Catalytic activity tests were performed at a synthesis gas (H_2/N_2 = 3/1) flow rate of 60 mL min^{-1} (STP) over 0.20 g of catalyst. The reaction temperature was varied from 588 to

653 K, and the pressure was varied from 0.1 to 1.1 MPa. The ammonia thus produced was trapped by a 2×10^{-3} N solution of sulfuric acid, and the rate of ammonia formation was determined from the decrease in the conductivity of the sulfuric acid solution. During the activity tests, the product gas flow was introduced to the sulfuric acid solution for measurement after a 30-min stabilization at each condition. The rate of ammonia synthesis reported herein is an average of three consecutive measurements over 60 min.

The stability of Ru/BHA was evaluated by conducting an extended reaction at 653 K and 0.1 MPa for 80 h.

2.4. Characterization

Several techniques were used to characterize the catalysts. The crystalline structure of the samples was analyzed by X-ray powder diffraction (XRD) (Multiflex S, Rigaku, Japan) using CuK_α radiation ($\lambda = 1.54050$ Å). All diffraction patterns were recorded in a 2θ range of 20°–70° at a scanning rate of 2° min^{-1} in steps of 0.02°. Brunauer–Emmett–Teller (BET) surface areas were measured on an automatic specific surface area/pore size distribution measurement apparatus (BELSORP-mini; BEL, Japan). Before adsorption tests, the samples were treated under a N_2 (99.9999%) flow at 423 K for 2 h.

The acidity of the supports was evaluated by temperature-programmed desorption (TPD) of ammonia in a laboratory-made glass vacuum system connected to a gas chromatograph (GC) (GC-8A, Shimadzu, Japan) equipped with a thermal conductivity detector (TCD). Before the desorption test, the sample (100 mg) was evacuated to 10^{-4} Pa at 973 K for 3 h, then cooled to 373 K under vacuum, and finally exposed to ammonia at ca. 1.3×10^4 Pa for 30 min, to allow the sample to reach adsorption equilibrium. The physically adsorbed ammonia molecules were then removed by evacuating to 10^{-4} Pa at 373 K for 30 min. In the desorption test, the sample was heated from 373 to 973 K at 10 K min^{-1}, and the desorbed ammonia was carried in He flow (50 mL min^{-1}) into the GC for quantification.

The number density of exposed Ru atoms on the catalysts was analyzed by an H_2-pulse titration method performed at 323 K assuming chemisorption stoichiometry of H:Ru = 1:1 [28,48,49]. Before measurements, the catalyst (50 mg) was heated under an Ar (99.9999%) flow at 25 mL min^{-1} for 30 min at 393 K, and then under a H_2 flow at 25 mL min^{-1} for 1 h at 473 K and a further 1 h at 723 K. The adsorbed H atoms on reduced samples were removed by purging with Ar (99.9999%) at 723 K for 10 min. After cooling to 323 K under Ar, H_2-pulse measurements were performed by repeatedly injecting 0.20 mL of 5 vol% H_2 in Ar (one pulse) at 323 K until a constant TCD response was achieved.

After H_2-chemisorption tests, the samples were observed by high-resolution field-emission transmission electron microscopy (HRTEM) (JEM-2010F, JEOL, Japan) at an accelerating voltage of 200 kV. The highest resolution achievable with this instrument was 0.19 nm. TEM samples were finely ground in an agate mortar, dispersed in isopropanol by sonication, and finally suspended on a carbon-coated copper grid. The composition of TEM samples was analyzed by energy-dispersive spectroscopy (EDS) (Noran Instruments, USA) as part of the TEM instrumentation. The smallest probe beam diameter achievable by this spectrometer was 0.5 nm.

The infrared (IR) spectra of adsorbed N_2 were collected by Fourier transform IR (FTIR) spectroscopy (Valor-III; JASCO Co., Japan) using a mercury–cadmium–tellurium detector. IR samples were pressed into self-supported disks (20 mm diameter) and then set in the center of a quartz IR cell [17]. The temperature of the samples was monitored using a thermocouple in a quartz tube mounted near the disks. The NaCl windows of the cell were sealed using Viton O-rings attached to aluminum flanges adhered to the cell with epoxy resin. The cell was connected to a closed gas circulation system. The samples were heated under vacuum at 723 K for 3 h, exposed for 12 h to circulated H_2 (27 kPa) purified using a liquid nitrogen trap, and then evacuated at the same temperature for 2 h to remove H_2. After pretreatment, the samples were cooled to 300 K under vacuum for acquisition of background spectra, then exposed to 27 kPa of N_2 for acquisition of IR spectra for N_2 adsorbed on the catalyst. The IR beam was adjusted to transmit through the center of samples. All spectra were scanned 64 times over a wavenumber range of 800–4200 cm^{-1} with 2 cm^{-1} resolution. Pure N_2 (99.9999%) and H_2 (99.9999%) were supplied to the system through a liquid nitrogen trap. Glass-bottled isotopic nitrogen ($^{15}N_2$, 99.8%) was used without purification.

3. Results

3.1. Catalytic performance of Ru/BHA

Table 1 compares the rates of ammonia synthesis over Ru catalysts supported on BHA, γ-Al_2O_3, and MgO. Among these samples, Ru/BHA achieved the highest rate of ammonia synthesis. At atmospheric pressure, the activity of Ru/BHA was more than twice that of either Ba–Ru/γ-Al_2O_3 or Ru/MgO, the latter of which was previously the most active known oxide support for Ru catalysts [32]. Although the 8 wt% Ru loading is somewhat higher than the optimum loading reported for the MgO support, the present rates are comparable to those reported for 5 wt% Ru/MgO [28].

The superiority of Ru/BHA was even more remarkable at higher pressure (Table 1). At 1.1 MPa, the activity of Ru/BHA was nearly three times of that of Ba–Ru/MgO, the second most-active catalyst among the samples tested. Such an increase in activity with pressure is contrary to the typical variation in ammonia synthesis rates over oxide-supported Ru catalysts, which decrease with increasing total reaction pressure. The decrease in activity, probably due to the stronger inhibition of H_2 at high pressures [20,24], was observed for Ru/γ-Al_2O_3, Ba–Ru/γ-Al_2O_3, and Ru/MgO (Table 1). The Ru/BHA system thus appeared to exhibit dissimilar behavior to previous Ru/oxide systems and generally higher activity for synthesis of ammonia.

The turnover frequencies (TOFs) for ammonia formation at active sites, calculated from the Ru dispersion expressed in terms of molar ratio of chemisorbed H to total Ru atoms, are summarized in Table 2. The apparent Ru dispersions of

Table 1
Rate of ammonia synthesis and BET specific surface area of 8 wt% Ru catalysts supported on various supports

Catalyst	BET surface area ($m^2\,g^{-1}$)	NH_3 synthesis rate at 0.1 MPa ($\mu mol\,g_{cat}^{-1}\,h^{-1}$)			NH_3 synthesis rate at 1.1 MPa ($\mu mol\,g_{cat}^{-1}\,h^{-1}$)		
		588 K	623 K	653 K	588 K	623 K	653 K
Ru/BHA	47 (45)	827	2267	3497	1202	3141	5426
Ru/γ-Al_2O_3	80	<100	<100	<100	<100	<100	<100
Ba–Ru/γ-Al_2O_3	64	446	1097	1897	328	895	1700
Ru/MgO	46 (24)	429	1109	2017	340	928	1920
Ba–Ru/MgO	57 (15)	293	735	1197	483	1326	2567

Ammonia synthesis conditions: 0.20 g catalyst, 60 mL min^{-1} (STP) synthesis gas ($N_2 + 3H_2$). Ba/Ru molar ratio is 1.6 for all the Ba-containing catalysts. Each rate of ammonia synthesis is determined as an average of three consecutive measurements over 60 min after 30-min stabilization under given conditions. Parentheses denote values for catalysts after reaction.

Table 2
Apparent dispersion of Ru and TOF for ammonia formation

Catalyst	H/Ru (%)	TOF ($\times 10^4$) at 0.1 MPa s^{-1}			TOF ($\times 10^4$) at 1.1 MPa s^{-1}		
		588 K	623 K	653 K	588 K	623 K	653 K
Ru/BHA	26.7	10.9	29.7	45.9	15.8	41.2	71.2
Ru/γ-Al_2O_3	33.5	1.0	1.0	1.0	1.0	1.0	1.0
Ba–Ru/γ-Al_2O_3	(33.5)	4.7	11.5	19.9	3.4	9.4	17.8
Ru/MgO	32.0	4.7	12.1	22.1	3.7	10.2	21.0
Ba–Ru/MgO	(32.0)	3.2	8.1	13.1	5.3	14.5	28.1

Note. Chemisorbed H_2 was zero for Ba-promoted catalysts. Dispersion values are thus calculated assuming that addition of Ba-promoters does not influence the size of Ru particles.

Ba–Ru/γ-Al_2O_3 and Ba–Ru/MgO could not be measured directly by the H_2-chemisorption method, because no H_2 was adsorbed by these catalysts at 323 K. We considered the Ru particles on these two samples to be completely covered by BaO species at 323 K. Thus, we used the Ru dispersion of the corresponding unpromoted catalysts (Ru/γ-Al_2O_3 and Ru/MgO) to calculate the TOF values for the Ba-promoted samples. The obtained results are considered reasonable because it has been reported that Ru dispersions are maintained on the addition of promoters when the catalysts are reduced under mild conditions [29,50,51]. The TOF for ammonia formation over Ru/BHA displayed generally the same trend as for the other catalyst systems, suggesting that the elevated activity of Ru/BHA was not due to a larger number density of exposed Ru atoms.

The stability of the catalyst system as another practically important factor can be determined from the change in the BET specific surface area of the catalysts during activity tests. The surface areas of the two MgO-supported catalysts decreased by >50% (Table 1) as a result of the activity tests for a time on steam of 20 h, consistent with previously reported results that MgO undergoes severe sintering under ammonia synthesis conditions [28,33]. The weight-specific activity of the MgO-supported catalysts indeed decreased with increasing time on stream. In contrast, the Ru/BHA catalyst exhibited a surface area decrease of <5%, from 47 to 45 $m^2\,g^{-1}$, indicating that Ru/BHA is morphologically more stable than Ru/MgO. This substantially improved morphological stability is further supported by the experimental results indicating that even after reaction for 80 h at 623 K and 0.1 MPa, the specific surface area of Ru/BHA remained as high as 44 $m^2\,g^{-1}$.

The change in the rate of ammonia synthesis over Ru/BHA with time is shown in Fig. 1. Catalyst deactivation was not observed during the 80-h test, whereas in our previous work, Ba-promoted Ru catalysts supported on active carbon exhibited a significant activity decrease with increased time on stream under conditions similar to those used in the present study [52]. The apparent Ru dispersion of the aged Ru/BHA obtained by H_2-chemisorption tests was ca. 37%, higher than that of the as-prepared sample (26.7%; Table 2). This noticeable increase in apparent Ru dispersion may be ascribed to the decreased coverage of Ru particles by Ba-rich species, as we discuss later. Nevertheless, the enhanced Ru dispersion demonstrates that the sintering of Ru particles did not occur in extended reactions,

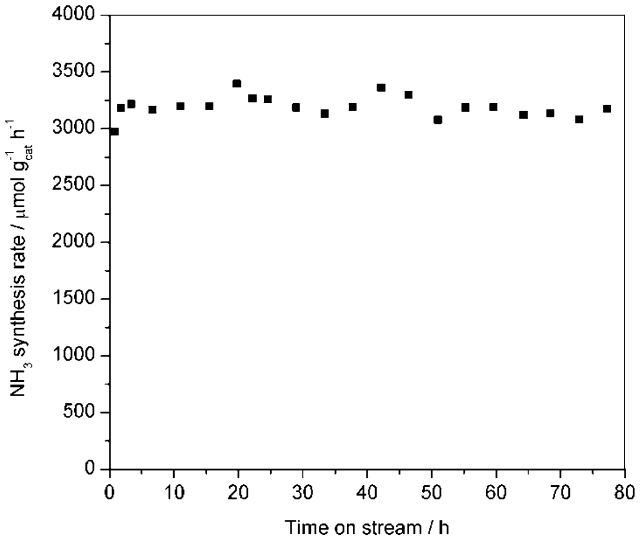

Fig. 1. Rate of ammonia synthesis over Ru/BHA vs time on stream. Reaction conditions: 0.20 g Ru/BHA, 60 mL min^{-1} (STP) synthesis gas ($N_2 + 3H_2$), 0.1 MPa, 653 K.

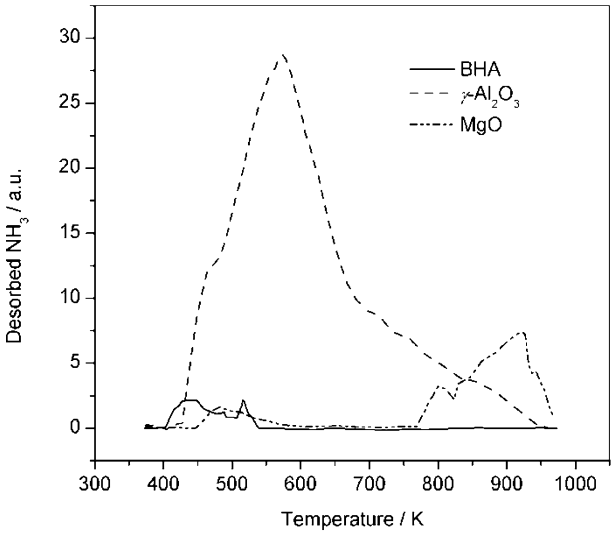

Fig. 2. Ammonia TPD profiles obtained over BHA, γ-Al_2O_3, and MgO. Samples (100 mg) were exposed to 13 kPa NH_3 at 373 K, and desorption was measured during heating at 10 K min^{-1} (He carrier gas, 50 mL min^{-1}).

Table 3
Ammonia adsorption by BHA, γ-Al_2O_3, and MgO

Support	BET surface area ($m^2\ g^{-1}$)	Adsorbed NH_3	
		(μmol g^{-1})	(μmol m^{-2})
BHA	49	5.4	0.11
γ-Al_2O_3	96	253.4	2.64
MgO	56	27.3	0.49

confirming the strength of the interaction between Ru particles and the BHA support.

3.2. Acidity of BHA

The strong acidity of oxide supports is known to be detrimental to the activity of Ru catalysts for ammonia synthesis. The surface acidity of the present supports determined by TPD of ammonia is shown in Fig. 2, and the amount of chemisorbed ammonia on these supports is given in Table 3. The amount of ammonia adsorbed on BHA was approximately 0.11 μmol m^{-2}, only 1/4 of that adsorbed on MgO (0.49 μmol m^{-2}), indicating that the number density of acid sites was much lower on BHA than on MgO. The acid strengths of these two supports, reflected by the desorption temperatures, were also very different. The NH_3 molecules bound to BHA desorbed at 400–550 K, approximately 400 K lower than for MgO. This difference suggests that the acid sites are much weaker on BHA than on MgO. Among the supports examined, γ-Al_2O_3 adsorbed the largest amount of ammonia (2.64 μmol m^{-2}) over a wide temperature range (400–950 K), consistent with the high density of strong acid sites known to be a characteristic of γ-Al_2O_3 [20,53]. In terms of acidity, BHA resembles alkaline earth oxide (i.e., BaO) instead of γ-Al_2O_3, although the content of Ba^{2+} is approximately 1/12 that of Al^{3+} in BHA, suggesting that the acidity of mixing oxides is more strongly related to structures than to compositions.

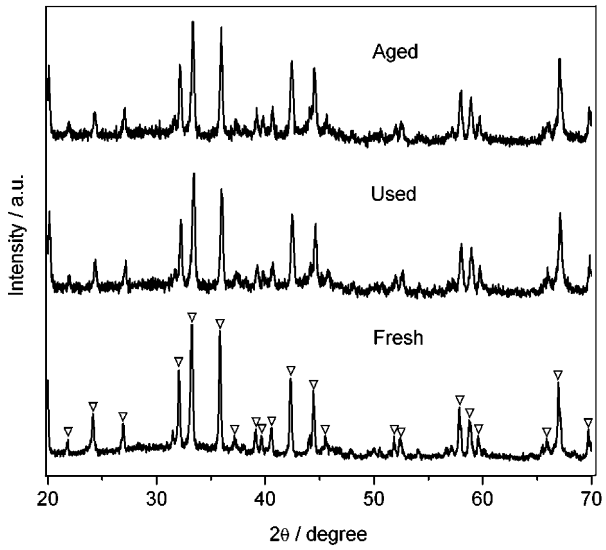

Fig. 3. XRD patterns for as-prepared Ru/BHA (fresh) and that after reaction tests (used) and extended reaction for 80 h (aged). Reaction conditions: 0.20 g Ru/BHA, 60 mL min^{-1} (STP) synthesis gas ($N_2 + 3H_2$), 0.1 MPa, 653 K. ($\triangledown$) $Ba_{0.75}Al_{11}O_{17.25}$.

3.3. Crystalline structure of BHA

Fig. 3 shows the XRD patterns of the as-prepared Ru/BHA catalyst and the catalysts after the activity test (used) and the extended reaction test (aged). All of the observable diffraction peaks can be assigned to the $Ba_{0.75}Al_{11}O_{17.25}$ phase. The diffraction patterns of the used and aged Ru/BHA catalysts remained the same as that for the fresh catalyst, indicating that the BHA structure was stable under these reaction conditions. The diffraction intensity of the used catalyst was slightly lower than for the as-prepared catalyst, suggesting minor degradation of crystallinity or superficial enrichment of heavy Ba atoms, which absorb incident X-rays and weaken the diffraction signals. However, no further decrease in diffraction intensity was observed after the extended reaction, demonstrating that the BHA support was structurally stable over long reactions. Despite the fact that the support was loaded with 8 wt% Ru, no diffraction peaks ascribed to Ru species were detected. This indicates either that the Ru particles were smaller in diameter than the detection limit (ca. 4 nm) of the diffractometer, or that large Ru particles (>4 nm) were too scarce to produce detectable diffraction signals. We discuss this result in more detail later.

The crystalline structure of BHA has been widely investigated [54–59]. According to Kimura et al. [58,59], the compound $BaAl_{12}O_{19}$ exists only as a mixture of two distinct nonstoichiometric phases, phase I ($Ba_{0.75}Al_{11}O_{17.25}$) and phase II ($Ba_{2.33}Al_{21.33}O_{34.33}$). The ideal structure of both phases is characterized by hexagonal symmetry with space group *$P6_3/mmc$*. The XRD results (Fig. 3) suggest that the microemulsion-derived BHA formed only the Ba-deficient phase I, consisting of spinel blocks of composition $[Al_{11}O_{16}]^+$ intercalated by mirror planes containing [BaO]. One unit cell of BHA consists of two spinel blocks and two mirror planes. Fig. 4a

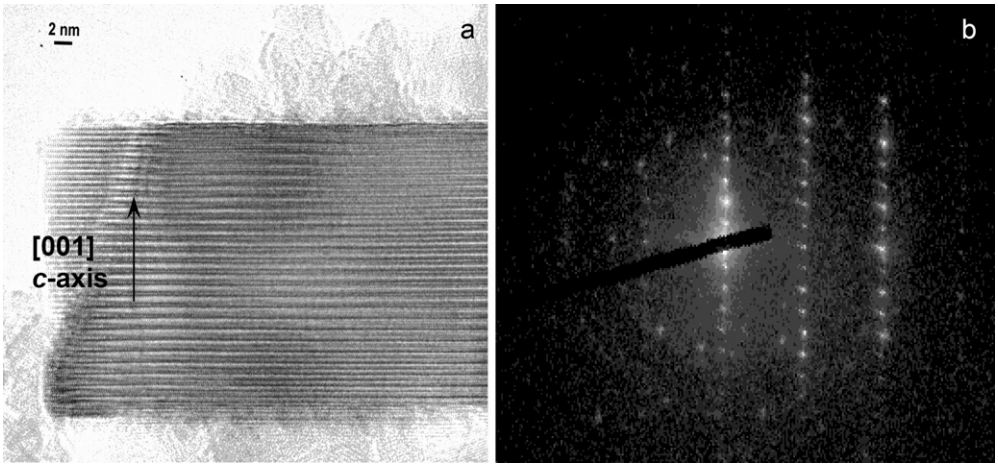

Fig. 4. (a) TEM image taken with incident electron beam oriented perpendicular to the *c*-axis of BHA crystal (calculated layer thickness: 11 Å), and (b) corresponding electron diffraction pattern.

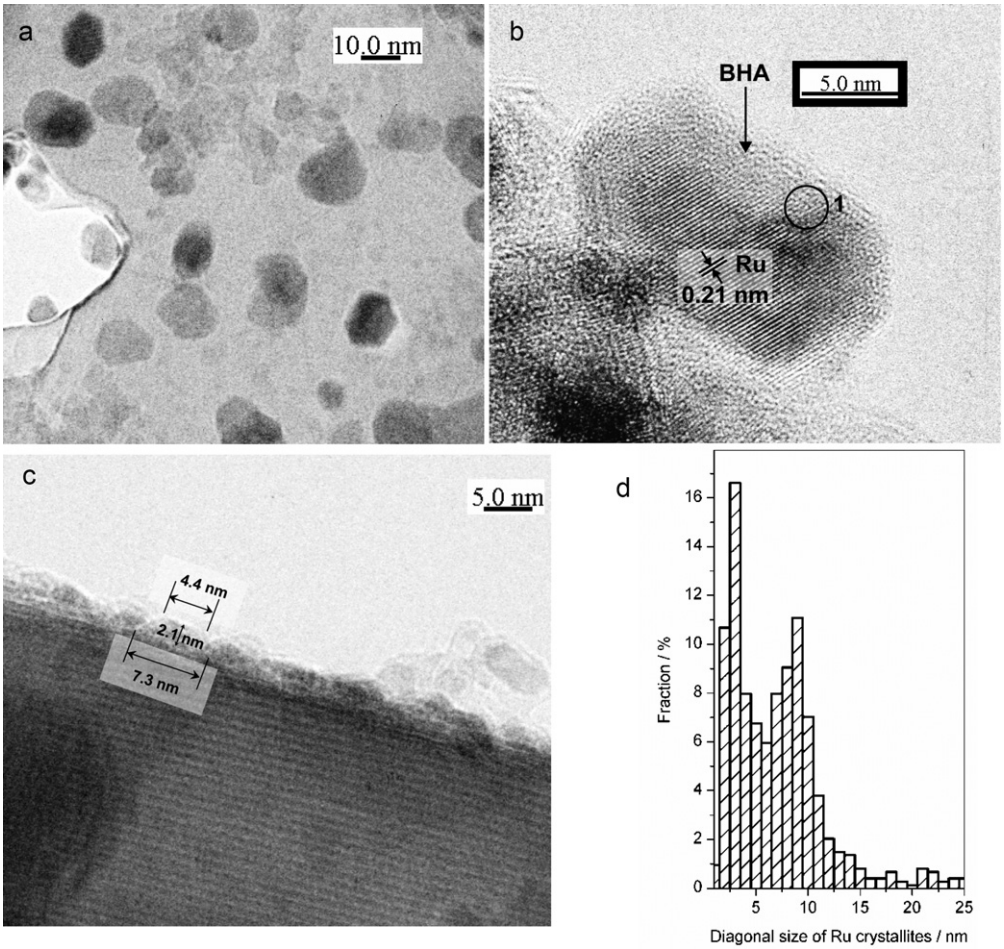

Fig. 5. (a) TEM image of Ru/BHA taken with incident electron beam oriented perpendicular to the (001) facet of BHA. (b) HRTEM image of Ru particle anchored on the edge of BHA support. EDS analysis was conducted for the encircled point. (c) TEM image of Ru/BHA taken with incident electron beam oriented parallel to the (001) facet of BHA. (d) Distribution of diagonal lengths of hexagonally shaped Ru crystallites (>500 Ru particles counted) on BHA.

shows the layered BHA structure formed by the present microemulsion synthesis. The thickness of one layer along the [001] direction of BHA, calculated from the electron diffraction pattern in Fig. 4b, was 1.1 nm, corresponding to half a unit cell.

3.4. Morphology of Ru particles supported on BHA

Fig. 5a shows the typical morphology of Ru particles on BHA after reduction by exposure to H_2 at 723 K for 2 h. Hexagonal-shaped ruthenium particles were uniformly de-

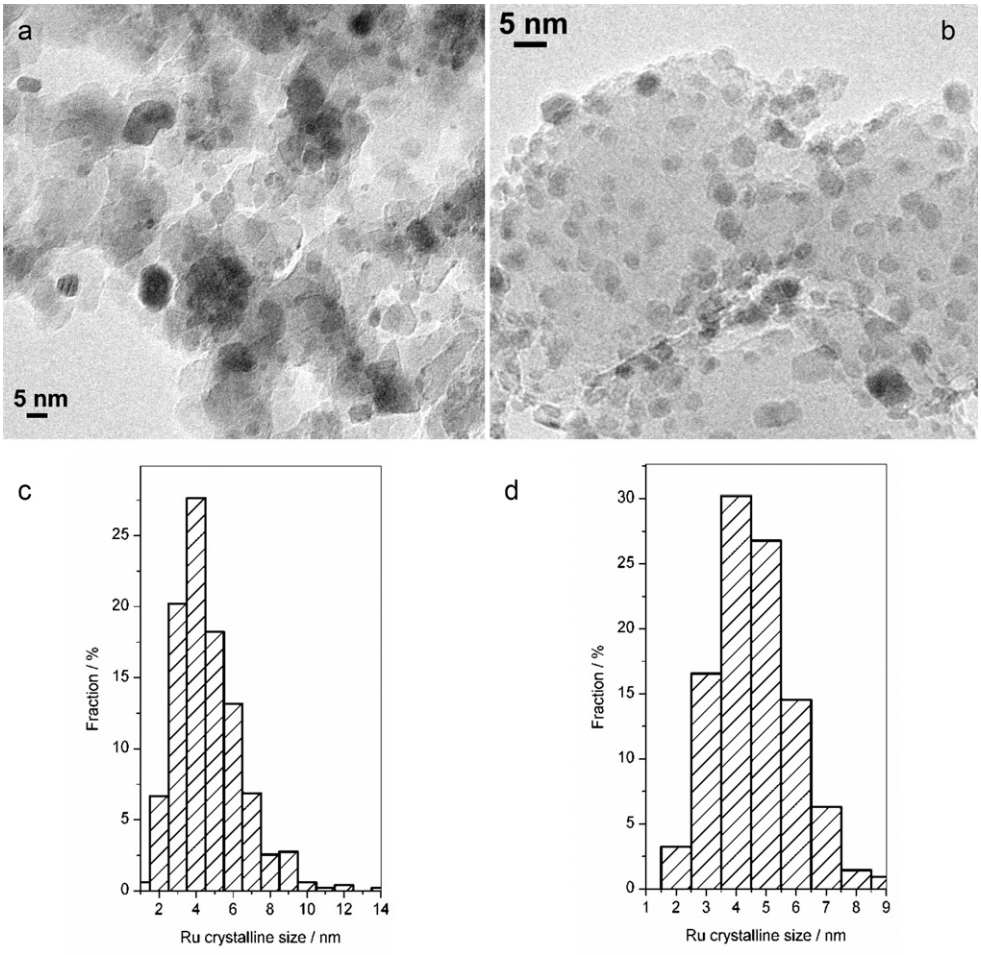

Fig. 6. TEM images of (a) Ru/γ-Al_2O_3 and (b) Ru/MgO, and (c, d) size distribution of Ru particles supported on (c) γ-Al_2O_3 and (d) MgO (>500 Ru particles counted).

posited on the (001) facets of the BHA substrate. The HRTEM image (Fig. 5b) shows a lattice spacing of Ru particles of 0.21 nm, corresponding to the (101) planes of Ru crystals [15,60]. The hexagonal shape and lattice spacing of Ru crystallites imply a (001) surface orientation of Ru particles on the BHA (001) facets. The TEM image in Fig. 5c, obtained with the incident electron beam oriented perpendicular to the [001] direction of BHA crystals, shows that all of the Ru crystallites grown on the (001) facets of the BHA substrate rose to a height of ca. 2 nm. Because the lattice parameter c of the Ru unit cells was 0.427 nm, the 2-nm height of the Ru particles corresponded to 5 unit cells or 11 hexagonally closely packed Ru (001) planes. The section of Ru particles projected normal to the [001] direction was trapezium-shaped, with parallel laterals approximately 4.4 and 7.3 nm long. Based on the projected shapes of Ru particles in the two perpendicular directions (Figs. 5a and 5c), most of the Ru particles on the BHA had a truncated hexagonal pyramid shape. The diagonal lengths of >500 Ru particles deposited on the (001) facets of the BHA measured from the TEM images are plotted in Fig. 5d. The diagonal lengths were bimodally distributed around 3 and 9 nm, indicating the presence of two types of Ru particles on the BHA support. The large particles are thought to form through the coalescence of smaller particles. The average diagonal length of Ru particles on the BHA was 7.45 nm.

The above TEM results also provide an explanation for the XRD results of Ru/BHA. Most Ru particles grown on BHA rose to a height of ca. 2 nm from the surface (Fig. 5c). Because this is smaller than the detection limit of the diffractometer, no diffraction peaks belonging to Ru could have been detected (see Fig. 3).

Fig. 5b shows that the Ru particles are surrounded by the BHA support. A similar partial coverage of Ru particles by supports has been observed for partially graphitized carbon [61,62] and BN [60] supports. The material in the region indicated by a circle in Fig. 5b was determined by EDS to have a Ba/Al ratio of 0.098, 44% greater than the value for bulk $Ba_{0.75}Al_{11}O_{17.25}$ (0.068). Thus, it appears that Ba^{2+} cations are enriched in this support material covering the edges of Ru particles. The EDS results are considered to reflect the appropriate composition of the covering material, because the selected Ru particle was anchored at the edge of the support and laid directly over a carbon-coated copper grid (not BHA).

The γ-Al_2O_3- and MgO-supported Ru catalysts exhibited very different morphologies than the Ru/BHA catalyst. Ruthenium particles on γ-Al_2O_3 were irregularly shaped, with an

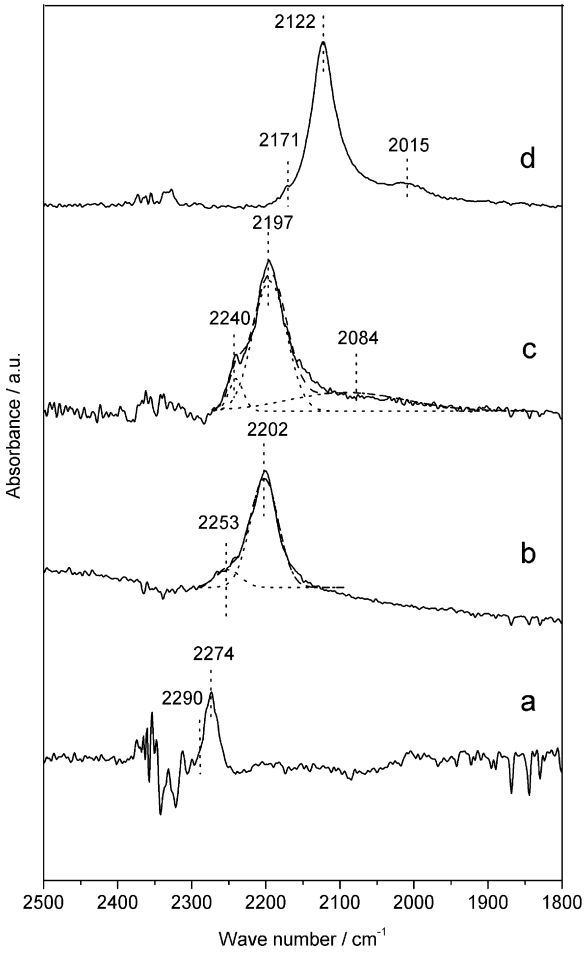

Fig. 7. Infrared spectra of N_2 molecules adsorbed on (a) Ru/γ-Al_2O_3 ($^{14}N_2$), (b) Ba–Ru/γ-Al_2O_3 ($^{14}N_2$), (c) Ru/BHA ($^{14}N_2$), and (d) Ru/BHA ($^{15}N_2$). Spectra were collected under 27 kPa of N_2 at 300 K.

average size of ca. 4.6 nm (Figs. 6a and 6c). Similar to Ru/BHA, the Ru particles supported on MgO appeared hexagonal in shape, but were equidimensional in size (Fig. 6b). MgO-supported Ru particles were more uniform than those on γ-Al_2O_3, although they had a similar average size of ca. 4.6 nm (Figs. 7c and 7d).

3.5. IR spectra of N_2 molecules adsorbed on Ru/BHA

The IR spectra of N_2 adsorbed on Ru/γ-Al_2O_3, Ba–Ru/γ-Al_2O_3, and Ru/BHA are shown in Fig. 7. In all spectra, noise peaks were present near 2340 cm^{-1}, attributed to the instability of atmospheric CO_2 concentration in the optical path. Ru/γ-Al_2O_3 exhibited a prominent IR absorption peak at 2274 cm^{-1} with a small shoulder at 2290 cm^{-1} (Fig. 8a). This main peak can be ascribed to N–N stretching at a frequency ca. 60 cm^{-1} higher than that observed for 2 wt% Ru/γ-Al_2O_3 [17]. According to Kubota and Aika [17], the frequency of the N–N stretching mode on Ru/γ-Al_2O_3 varies with the Ru particle size and pretreatment temperature. The Ru particles at the present loading (8 wt%) would be much larger than those at 2 wt% Ru, and samples in this study were also pretreated at lower temperature (723 K). Thus, both of these factors likely influenced the

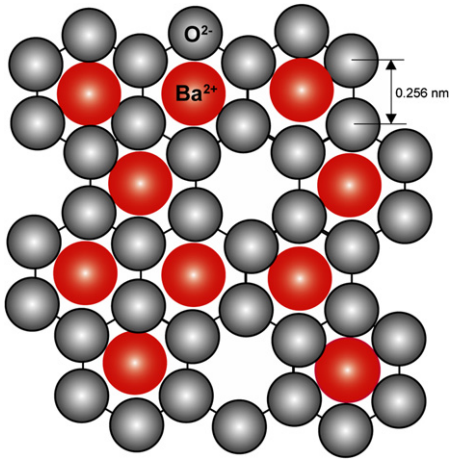

Fig. 8. Model of exposures of BaO-containing mirror planes on BHA surface.

frequency of this absorption peak. The small shoulder located at 2290 cm^{-1} presumably is associated with N_2 molecules adsorbed on positively charged Ru atoms [17]. After the Ba promoter was added to Ru/γ-Al_2O_3, the two IR absorption bands shifted to lower frequencies (the main band to 2202 cm^{-1} and the shoulder to 2253 cm^{-1}), revealing weakening of the N–N bonds by the Ba promoter. In the case of Ru/BHA, three IR bands were observed at 2240, 2197, and 2084 cm^{-1}. The main peak at 2197 cm^{-1} is attributed to the stretching mode of on-top N–N, and the shoulder at 2240 cm^{-1} is assigned to N_2 molecules adsorbed on positively charged Ru atoms. The occurrence of these two peaks at slightly lower frequencies compared with Ba–Ru/γ-Al_2O_3 suggests that the Ba^{2+} cations in the lattice of BHA exhibited the same or even stronger promoter effects. A more interesting result is that Ru/BHA gave a third broad absorption peak located at 2084 cm^{-1}, which was not observed for Ba–Ru/γ-Al_2O_3. This peak was too broad and weak to allow clear identification. To clarify this ambiguous peak, the IR spectrum of $^{15}N_2$ on Ru/BHA was obtained (Fig. 8d). By the isotopic effect, where the frequency of this peak was shifted to 2015 cm^{-1}, in good agreement with the theoretical value of $2084/(15/14)^{1/2} = 2013$ cm^{-1}, the presence of the third peak undoubtedly represents N_2 molecules three-fold adsorbed on B_5 sites at the side facets, as we discuss later.

4. Discussion

4.1. Electronic promotion effect of BHA

The ideal surface for an ionic oxide is a plane exposed by cutting a larger crystal, where the plane is constituted by coordinately unsaturated metal and oxygen centers. Such centers are labile due to their high free energy, causing the surface to reorganize and react with environmental molecules (e.g., water and CO_2) until the surficial free energy reaches a minimum. Thus, the real surface of an ionic oxide is likely to contain cationic centers (potentially acting as Lewis acid sites), oxide anionic species (potentially acting as basic sites), hydroxyl groups formed from dissociative adsorption of water (potentially acting as Brønsted acid sites or basic sites), and other sur-

face species arising from reactions with environmental molecules, such as carbonate. Theoretically, any ionic oxide has both acidic and basic sites at its surface. The nature of oxide surfaces is ultimately governed by the relative strength of all of these exposed acidic or basic centers.

Among these sites, Lewis acid centers are the most detrimental to ammonia synthesis due to the consumption of electrons of Ru atoms as an interaction between the support and the Ru particles. The strength of Lewis acid sites is related to the polarization power (cationic charge/ionic radius) of cations. Small cations with high valence, such as Al^{3+}, have high polarization power and strong Lewis acidity, whereas large cations with low valence, such as Mg^{2+} and Ba^{2+}, have low polarization power and weak Lewis acidity. Busca [53] has reported that the polarization power of BaO is 1.48, 40% of that for MgO (3.7) and 20% of that for γ-Al_2O_3 (7.7). The strength of Lewis acidity should thus decrease in the order γ-$Al_2O_3 \gg$ MgO > BaO (BHA), which is in good agreement with the present ammonia TPD results.

BHA has a layered structure (see Fig. 4), in which alumina spinel blocks are intercalated by mirror planes containing [BaO] [55]. γ-Al_2O_3 also constitutes defective spinel blocks, and in this respect the structures of BHA and γ-Al_2O_3 bear some resemblance. However, during formation of the BHA phase, the exposed surface consists of [BaO]-containing mirror planes [54], which constrain growth in the *c*-axis direction of the BHA crystals to afford an anisotropic layered structure. This anisotropic growth feature endows BHA with high thermal stability, contributing to the textural stability of the Ru/BHA observed in this work.

Besides having a stabilizing effect, the [BaO]-containing mirror planes also form a shield for the spinel blocks in the BHA. Such a structural configuration provides BHA with similar surface acidity to that of BaO, very different from the case of γ-Al_2O_3, which explains the low density and strength of acid sites on BHA compared with MgO and γ-Al_2O_3 (Fig. 2 and Table 3). Thus, BHA would be expected to exhibit a strong electron-donation capacity comparable to that of BaO, which has proven to be a very active promoter for Ru catalysts. This effect must be one of the main factors responsible for the superior catalytic performance of Ru/BHA.

4.2. Structural promotion effect of BHA

The peculiar layered structure of BHA contributes to the elevated activity of Ru/BHA not only in terms of electronic interactions, but also by structural effects. The Ru/C catalyst is known to be the most active catalyst for ammonia synthesis, due primarily to the effect of the graphitization and texture of the carbon support. Song et al. [15] confirmed the structural promotion effect of graphitized carbon by scanning tunneling microscopy (STM), revealing that flat Ru particles grown epitaxially on the surface of graphitized carbon hosted more B_5 sites and exhibited more surface strain than round particles. In this work, we found that the layered structure of BHA also induced the epitaxial growth of flat Ru particles in a manner similar to graphitized carbon. As revealed by XRD measurements (Fig. 3), the microemulsion-derived BHA is composed mainly of Ba-deficient phase I ($Ba_{0.75}Al_{11}O_{17.25}$), which has a β-alumina structure ($NaAl_{11}O_{17}$) with Na^+ cations replaced by Ba^{2+}. Substitution of monovalent Na^+ with divalent Ba^{2+} resulted in replacement of 1/4 of the Ba^{2+} in mirror planes (Beevers–Ross sites) with O^{2-} (Reidinger defects) to maintain electroneutrality [58]. The exposed mirror planes of BHA constitute mainly hexagonally close-packed oxide anions and some Ba cations in the interstices, as illustrated in Fig. 8. The hexagonally close-packed oxygen anions can induce the epitaxial growth of Ru crystallites in a manner similar to the hexagonally close-packed carbon atoms of graphite reported by Song et al. [15]. Given the nearest-neighbor atom distance on the Ru (001) surfaces (0.271 nm) and on the mirror planes of BHA (0.256 nm), the mismatch of the Ru (001) lattice with respect to the hexagonal structure of the oxygen lattice is 5.9%.

Fig. 5a, a TEM image obtained with the incident electron beam oriented perpendicular to the (001) surface, clearly shows that most of the Ru particles on the (001) surface of BHA are hexagonal. Unlike STM, obtaining three-dimensional information on objects by TEM is not easy. Thus, in this study, the heights of the Ru particles were determined by observing the sample with the incident electron beam oriented parallel to the (001) surface (Fig. 5c), which revealed trapezium-shaped particles ca. 2 nm in height. Although these TEM results are insufficient evidence to indicate that most Ru particles on the BHA are flat, the lack of XRD peaks assignable to Ru species in Ru/BHA (indicating a particle height of <4 nm) and the large average projected diagonal length (7.3 nm) of Ru particles on the (001) surface of BHA suggest that the Ru particles are considerably flat.

Based on these results, the proposed model of the morphology of Ru particles grown epitaxially on the BHA support is shown in Fig. 9a. The calculated Ru dispersion for this model is ca. 30%, 3% greater than the measured value obtained by H_2 chemisorption (Table 2). Taking into account the coverage of Ru atoms by Ba-rich species (Fig. 5b), the Ru dispersion calculated from the proposed model can be considered reasonable, indicating that the proposed model accurately reflects the average situation of Ru particles supported on BHA.

The average height of particles is ca. 2 nm, equivalent to 11 layers of Ru atoms. Thus, the surface Ru atoms on flat Ru particles are closer to the BHA surface than the thicker Ru particles on MgO and γ-Al_2O_3 (Fig. 6), allowing stronger electrostatic interactions with the support. These structural features may be responsible for the downward shift in the frequency of N–N stretching for Ru/BHA compared with Ba–Ru/γ-Al_2O_3 (Figs. 8b and 8c).

The six side facets of the Ru particles with a truncated hexagonal pyramidal shape are composed of steps (Fig. 9b). Thus, the density of B_5 sites on these side facets is likely to be substantially greater than that for round particles. The adsorption of N_2 molecules at B_5 sites is considered to be threefold adsorbed [37], resulting in weaker N–N bonds than those for onefold adsorbed N_2 molecules. Thus, IR photons absorbed by such weakened N–N bonds will appear at lower frequency. It seems reasonable to ascribe the broad IR absorption band at

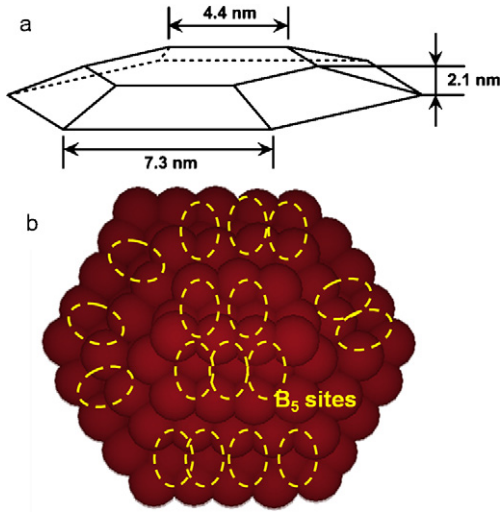

Fig. 9. (a) Proposed model of flat Ru crystallites with truncated hexagonal pyramid shape on BHA. (b) Ball model illustrating the many steps and B_5 sites on the side facets of flat Ru crystallites grown epitaxially on the BHA (001) surface.

2084 cm^{-1} in Fig. 7c to N_2 molecules threefold adsorbed at B_5 sites on the side facets. If this assignment is correct, then the percentage of B_5 sites relative to the total sites that adsorb N_2 molecules can be calculated as ca. 40%. The area of the 2084 cm^{-1} peak is ca. 40% of the total area after deconvolution of the three Gaussian-type IR peaks shown in Fig. 7c, corresponding to the areal proportion of B_5 sites to total exposed Ru atoms on the catalyst surface.

Similar to the situation described by Song et al. [15], dislocations should exist on the surface and in the bulk of the flat Ru particles on BHA, and such dislocation could induce surface strain. Nitrogen coverage in the stretched area of a strained surface is known to be much higher than in unstrained areas [63], and this effect is considered responsible for the elevated activity of flat Ru particles for N_2 dissociative adsorption.

5. Conclusion

Barium hexaaluminate with a large surface area was prepared by microemulsion-mediated synthesis and examined as a support promoting ammonia synthesis catalyzed by particulate Ru. The Ru/BHA system exhibited markedly higher activity and stability for ammonia synthesis compared with Ba-promoted Ru on an MgO support, which was previously considered the most active oxide support for this reaction. The superior performance of Ru/BHA can be attributed primarily to the peculiar layered structure of BHA, which has a similar structural promotion effect to that of graphitized carbon, whereby the (001) facet of BHA induces the epitaxial growth of flat Ru particles with truncated hexagonal pyramid shape. The microemulsion-derived BHA has been found to consist of the $Ba_{0.75}Al_{11}O_{17.25}$ phase, which has a structure comprised of spinel blocks intercalated by [BaO]-containing mirror planes. The surficial layer of BHA is a [BaO]-containing mirror plane, which endows BHA with an electronic-promoting effect similar to that BaO. Thus, BHA combines the electronic advantages of alkaline earth oxides and the structural advantages of graphitized carbon to provide an excellent support for Ru as a catalyst for ammonia synthesis.

Acknowledgments

Financial support was provided by the Ministry of Education, Culture, Sports, Science, and Technology of Japan (Grant 14205115). This work was also supported by the Core Research for Evolutional Science and Technology (CREST) program of the Japan Science and Technology Agency (JST).

References

[1] A. Ozaki, K. Aika, Catalysis—Science and Technology, in: J.R. Anderson, M. Boudart (Eds.), vol. 3, Springer-Verlag, Berlin, 1981, p. 139.
[2] S.R. Tennison, in: J.R. Jennings (Ed.), Catalytic Ammonia Synthesis: Fundamentals and Practice, Plenum, New York, 1991.
[3] C.J.H. Jacobsen, Chem. Commun. (2001) 1057.
[4] K. Aika, M. Hori, A. Ozaki, J. Catal. 27 (1972) 424.
[5] K. Aika, A. Ohya, A. Ozaki, Y. Inoue, I. Yasumori, J. Catal. 92 (1985) 305.
[6] S. Murata, K. Aika, Appl. Catal. A 82 (1992) 1.
[7] K. Aika, K. Tamaru, in: A. Nielsen (Ed.), Ammonia: Catalysis and Manufacture, Springer-Verlag, Berlin, 1995, chap. 3.
[8] F. Rosowski, O. Hinrichsen, M. Muhler, G. Ertl, Catal. Lett. 36 (1996) 229.
[9] O. Hinrichsen, F. Rosowski, A. Hornung, M. Muhler, G. Ertl, J. Catal. 165 (1997) 33.
[10] B.C. McClain, R.J. Davis, J. Catal. 210 (2002) 387.
[11] C.J.H. Jacobsen, J. Catal. 200 (2001) 1–3.
[12] K. Aika, K. Shimazaki, Y. Hattori, A. Ohya, S. Ohshima, K. Shirota, A. Ozaki, J. Catal. 92 (1985) 296.
[13] US patent 4 163 775, 1979, to British Petroleum.
[14] C. Liang, Z. Li, J. Qiu, C. Li, J. Catal. 211 (2002) 278.
[15] Z. Song, T. Cai, J.C. Hanson, J.A. Rodriguez, J. Hrbek, J. Am. Chem. Soc. 126 (2004) 8576.
[16] O. Hinrichsen, F. Rosowski, M. Muhler, G. Ertl, Chem. Eng. Sci. 51 (1996) 1683.
[17] J. Kubota, K. Aika, J. Phys. Chem. 98 (1994) 11293.
[18] S. Murata, K. Aika, J. Catal. 136 (1992) 118.
[19] K. Aika, M. Kumasaka, T. Oma, O. Kato, H. Masuda, N. Watanabe, K. Yamazaki, A. Ozaki, T. Onishi, Appl. Catal. 28 (1986) 57.
[20] Y. Kadowaki, K. Aika, J. Catal. 161 (1996) 178.
[21] J. Wellenbuscher, M. Muhler, W. Mahdi, U. Sauerlandt, J. Schütze, G. Ertl, R. Schlögl, Catal. Lett. 25 (1994) 61.
[22] K. Chao, L. Lin, M. Yang, Catal. Lett. 38 (1996) 279.
[23] C.T. Fishel, R.J. Davis, J.M. Garces, J. Catal. 163 (1996) 148.
[24] Y. Niwa, K. Aika, J. Catal. 162 (1996) 138.
[25] B. Fastrup, Catal. Lett. 48 (1997) 111.
[26] D. Szmigiel, W. Raróg-Pilecka, E. Miśkiewicz, E. Maciejewska, Z. Kaszkur, J.W. Sobczak, Z. Kowalczky, Catal. Lett. 100 (2005) 79.
[27] L. Forni, D. Molinari, I. Rossetti, N. Pernicone, Appl. Catal. A 185 (1999) 269.
[28] F. Rosowski, A. Hornoung, O. Hinrichsen, D. Herein, M. Muhler, G. Ertl, Appl. Catal. A 151 (1997) 443.
[29] Z. Kowalczyk, S. Jodzis, W. Raróg, J. Zieliński, J. Pielaszek, Appl. Catal. A 173 (1998) 153.
[30] P.J. Goethel, P.T. Yang, J. Catal. 111 (1988) 220–226.
[31] Z. Kowalczyk, J. Sentek, S. Jodzis, R. Diduszko, A. Presz, A. Terzyk, Z. Kucharski, J. Suwalski, Carbon 34 (1996) 403.
[32] S. Dahl, J. Sehested, C.J.H. Jacobsen, E. Törnqvist, I. Chorkendorf, J. Catal. 192 (2000) 391.
[33] K. Aika, T. Takano, S. Murata, J. Catal. 136 (1992) 126.
[34] O. Hinrichsen, Catal. Today 53 (1999) 177.

[35] C.J.H. Jacobsen, S. Dahl, P.L. Hansen, E. Törnqvist, L. Jensen, H. Topsøe, D.V. Prip, P.B. Møenshaug, I. Chorkendorf, J. Mol. Catal. A 163 (2000) 19.
[36] S. Dahl, P.A. Taylor, E. Tornqvist, I. Chorkendorf, J. Catal. 178 (1998) 679.
[37] S. Dahl, A. Logadottir, R.C. Egeberg, J.H. Larsen, I. Chorkendorf, E. Törnqvist, J.K. Nørskov, Phys. Rev. Lett. 83 (1999) 1814.
[38] S. Dahl, E. Tornqvist, I. Chorkendorf, J. Catal. 192 (2000) 381.
[39] T.W. Hansen, P.L. Hansen, S. Dahl, C.J.H. Jacobsen, Catal. Lett. 84 (2002) 7.
[40] T. Komaya, A.T. Bell, Z. Weng-Sieh, R. Gronsky, F. Engelke, T.S. King, M. Pruski, J. Catal. 149 (1994) 142.
[41] C. Liang, Z. Wei, Q. Xin, C. Li, Appl. Catal. A 208 (2001) 193.
[42] T. Hikita, Y. Kadowaki, K. Aika, J. Phys. Chem. 95 (1991) 9396.
[43] Á. Logadóttir, J.K. Nørskov, J. Catal. 220 (2003) 273.
[44] I. Balint, Z. You, K. Aika, Phys. Chem. Chem. Phys. 4 (2002) 2501.
[45] Z. You, I. Balint, K. Aika, Chem. Lett. 32 (2003) 630.
[46] Z. You, I. Balint, K. Aika, Chem. Lett. 31 (2002) 1090.
[47] Z. You, K. Inazu, I. Balint, K. Aika, Chem. Lett. 34 (2005) 692.
[48] R.A.D. Betta, J. Catal. 34 (1974) 57.
[49] K.C. Taylor, J. Catal. 38 (1975) 229.
[50] T.W. Hansen, P.L. Hansen, S. Dahl, C.J.H. Jacobsen, Catal. Lett. 84 (2002) 7.
[51] W. Raróg-Pilecka, E. Miśkiewicz, D. Szmigiel, Z. Kowalczyk, J. Catal. 231 (2005) 11.
[52] H.S. Zeng, K. Inazu, K. Aika, J. Catal. 211 (2002) 33.
[53] G. Busca, Phys. Chem. Chem. Phys. 1 (1999) 723.
[54] G. Groppi, F. Assandri, M. Bellotto, C. Cristiani, P. Forzatti, J. Solid State Chem. 114 (1995) 326.
[55] M. Machida, A. Sato, M. Murakami, T. Kijima, H. Arai, J. Catal. 157 (1995) 713.
[56] S. Kimura, E. Bannai, I. Shindo, Mater. Res. Bull. 17 (1982) 209.
[57] N. Yamamoto, M. O'Keeffe, Acta Crystallogr. Sect. B Struct. Sci. 40 (1984) 21.
[58] N. Iyi, Z. Inoue, S. Takekawa, S. Kimura, J. Solid State Chem. 52 (1984) 66.
[59] N. Iyi, Z. Inoue, S. Takekawa, S. Kimura, J. Solid State Chem. 60 (1985) 41.
[60] H. Topsøe, J.B. Wagner, P.L. Hansen, S. Dahl, T.W. Hansen, C.J.H. Jacobsen, Science 294 (2001) 1508.
[61] Z. Kowalczyk, S. Jodzis, W. Raróg, J. Zieliński, J. Pielaszek, A. Presz, Appl. Catal. A 184 (1999) 95.
[62] Z. Kowalczyk, J. Sentek, S. Jodzis, R. Diduszko, E. Mizera, J. Góralski, T. Paryjczak, Catal. Lett. 45 (1997) 65.
[63] J. Wintterlin, T. Zambelli, J. Trost, J. Greeley, M. Mavrikakis, Angew. Chem. Int. Ed. 42 (2003) 2850.